Available online at www.sciencedirect.com

ScienceDirect

Ceramics International 40 (2014) 437–445

CERAMICS INTERNATIONAL

www.elsevier.com/locate/ceramint

Influence of substrate temperature on the properties of CeO_2 thin films by simple nebulizer spray pyrolysis technique

R. Suresh[a], V. Ponnuswamy[a,*], R. Mariappan[a,b], N. Senthil Kumar[a]

[a]Department of Physics, Sri Ramakrishna Mission Vidyalaya College of Arts and Science, Coimbatore 641020, Tamilnadu, India
[b]Department of Physics, Adhiyamaan College of Engineering, Hosur-635109, Tamilnadu, India

Received 23 March 2013; received in revised form 24 May 2013; accepted 10 June 2013
Available online 21 June 2013

Abstract

Cerium oxide thin films are coated on glass substrates by nebulizer spray pyrolysis technique using cerium nitrate as a source material. Their crystallographic structures, surface morphology, optical properties and *I–V* characteristics are studied as a function of substrate temperature (300–500 °C). XRD is used to estimate the crystallographic texture, grain size, strain and lattice constants. All the films exhibit a cubic fluorite structure with different preferred orientations depending on the preparation conditions. Optical analysis reveals that the films are transparent (70%) in the visible region. The optical bandgap (E_g) is calculated in the range 3.28–3.52 eV. The optical parameters like absorption coefficient, extinction coefficient, packing density and refractive index are calculated for different substrate temperatures. SEM images exhibit golf-ball like morphology with small cracks and pores. The maximum conductivity obtained is 2.90×10^{-6} S/cm at 400 °C.

Keywords: C. Electrical properties; C. Optical properties; Thin films; X-ray diffraction

1. Introduction

Cerium has low toxicity and is relatively abundant in nature. Cerium compounds are good cathodic inhibitors as they show more negative potential values. It has an affinity for oxygen and the bonding between cerium and oxygen is unlikely to be broken under the cathodic potential region [4]. It has been one of the technologically most important oxide materials owing to its well-known redox chemistry, chemical stability and close lattice parameter with silicon [1]. It is a wide band gap rare earth material with a band gap value 3.6 eV at room temperature [2]. It exhibits two structures mainly cubic fluorite cerium dioxide or ceria (due to tetravalent Ce) and a hexagonal sesquioxide Ce_2O_3 (due to trivalent Ce) [3]. CeO_2 is a notable functional material with an extraordinary capacity to store and release oxygen while preserving its fluorite cubic structure. It has been commonly used as an additive or support material in oxidation catalysts, because of the ability to act as intermediate oxygen storage media and as noble metal dispersion aid, as well as high temperature stabilizer. In the past decades, CeO_2-based materials have been widely studied as catalyst supporters and promoters for heterogeneous catalytic reactions. SOFC's have attracted increasing attention in scientific community because of their remarkable advantages like long-term stability and economical competitiveness for some vehicles and stationary applications. Pure and doped CeO_2 thin films have been widely used in the fields of corrosion inhibitors [4], semiconductors [5], gas sensors [6,7], electrochromic devices [8], counter electrodes [3,9,10], high-temperature superconductors [11,12] and SOFC [13–19].

Several methods have been proposed to prepare cerium oxide thin films such as Chemical Vapor Deposition (CVD) [20], Pulsed Laser Deposition [21,22], Dip coating [23], Electrostatic Spray Assisted Vapor Deposition (ESAVD) [24], Pulsed Spray Evaporation Chemical Vapor Deposition (PSE-CVD) [25], Electron Beam Evaporation and Ion Beam Assisted Deposition (EBE-IBAD) [26], Electron Beam Physical Vapor Deposition (EB-PVD) [6,27], Flame Spray [28] and spray pyrolysis [1,2,29–33,36]. Among these methods, spray pyrolysis is the simple, low cost and reliable process to

*Corresponding author. Tel.: +91 4222 69 2461; fax: +91 4222 69 3812.
E-mail addresses: ponns007@yahoo.com, rsdphy@gmail.com (V. Ponnuswamy).

0272-8842/$ - see front matter © 2013 Elsevier Ltd and Techna Group S.r.l. All rights reserved.
http://dx.doi.org/10.1016/j.ceramint.2013.06.020

produce uniform and well adherence films. It has been widely used to produce fine powders because it is a continuous and ambient pressure process. It consists of three successive steps: (i) atomization of a liquid precursor containing metal salts, (ii) droplet transport towards a heated substrate and film formation of the substrate surface and (iii) evaporation of the solvent and decomposition of the deposited material. Crack-free films can be obtained when deposition temperature is above precursor boiling point. In this method, substrate temperature plays an important role in film formation. This technique has some advantages: (i) it has the capacity to produce large area high quality films of uniform thickness, (ii) the addition of dopants to the spray solution is simple, and (iii) it is easy to prepare films of any composition by simply mixing the components in the appropriate ratios [13].

In the present work an attempt has been made to investigate the crystallographic structures, surface morphology, optical properties and electrical properties as a function of substrate temperature of the films prepared by the nebulizer spray pyrolysis method using cerium nitrate as the source material.

2. Experimental details

Cerium oxide (CeO_2) thin films are deposited on glass substrates using cerium nitrate hexahydrate as the chemical precursor. The substrates are cleaned using hydrochloric acid, sodium hydroxide, isopropyl alcohol and then rinsed with deionized water. 0.02 M of cerium nitrate is dissolved in 50 ml of deionized water and stirred for 30 min. The prepared solution is deposited on glass substrates using jet nebulizer. The compressed air is used as the carrier gas. The substrate temperature is varied from 300 to 500 °C. Nozzle–substrate distance is fixed at 5 cm. The aerosol formed from nozzle undergoes successive pyrolysis due to temperature gradient and successive pyrolysis results into decomposition of aerosol at substrate and leads to film formation. The substrate temperature is fixed at 300 °C slightly higher than that of decomposition temperature (290 °C) of the precursor solution. The prepared samples are characterized by UV–vis, XRD, SEM, EDAX and *I–V* characteristics.

Optical characterization of thin film is mainly done with the help of optical spectrophotometers by taking absorbance, transmittance and reflectance in a range of wavelength. In the present work, optical properties of thin films are analyzed using a JASCO spectrometer instrument. Thickness is calculated using a surface profilometer. In order to understand the properties of materials, deep knowledge about the structure and their composition is important. X-ray Diffraction (XRD) is a powerful technique used to identify the crystalline phases present in materials and measure the structural properties (strain state, grain size, epitaxy, phase composition, preferred orientation, and defect structure) of these phases. Samples are analyzed by a XPERT-PRO Bruker AXS D8 advanced X-ray diffractometer in the 0–90° (2θ) scale angle range. Also, the thin film samples are analyzed using JEOL Model JSM-6390LV instrument for high resolution surface imaging. Energy Dispersive X-Ray Spectroscopy (EDS or EDX) is a chemical microanalysis technique used in conjunction with scanning electron microscopy (SEM). The EDS technique detects X-rays emitted from the sample during bombardment by an electron beam to characterize the elemental composition of the analyzed volume using JEOL Model JED-2300 instrument. *I–V* characteristics are analyzed with the help of Keithley electrometer 6517B. XPS is a straightforward and nondestructive technique for the investigation of chemical and electronic structures of materials. XPS measurements on CeO_2 films were carried out by using a VG Microtech Multilab ESCA 3000 spectrometer.

3. Results and discussion

3.1. Optical properties

The variations of transmittance, absorbance and reflectance of cerium oxide thin films with wavelength in the range 300–900 nm are shown in Fig. 1a–c. It shows that the transmittance decreases to zero in the UV region and increases to 70% in the visible region, but the absorbance has a very high value in the UV region and decreases sharply with increasing wavelength and becomes almost constant towards the visible region [34]. The low transmittance is probably due to the existence of an interfacial layer with high refractive index between CeO_2 and glass. It is observed that (Fig. 1c) the reflectance of the films shifts towards higher wavelength side with the temperature also increased. Bandgap values are obtained by extrapolation of the linear region of higher photon energy to zero absorption coefficient using linear fits close to the absorption edge as shown in Fig. 1d. The optical absorption coefficient (α) was evaluated from the transmission spectra. The variation α with photon energy ($h\nu$) was found to obey this relation:

$$\alpha = \frac{\ln(1/T)}{t} \tag{1}$$

$$(\alpha h\nu)^{1/2} = B(h\nu - E_g) \tag{2}$$

where t is the film thickness, A is a constant, E_g is the optical band gap energy and α is related to the extinction coefficient k by

$$k = \frac{\alpha\lambda}{4\pi} \tag{3}$$

The optical band gap values are obtained by extrapolating the linear portion of the plots of $(\alpha h\nu)^2$ with $h\nu$ of the films formed at different substrate temperatures from 300 to 500 °C which are shown in Fig. 1d. The optical band gap of the CeO_2 films are found to be increased from 3.35 to 3.50 eV with the temperature increasing from 300 to 400 °C. These values of optical band gap are in good agreement with the reports [26]. The absorption $(\alpha)t$ of CeO_2 films as the function of wavelength in the range 300–900 nm is shown in Fig. 2a. It is observed that Fig. 2a the absorption coefficient of the films decreases sharply with the temperature. It is clear from Fig. 2b that the extinction coefficient (k) has its minimum value at lower energy and increases with increasing photon energy.

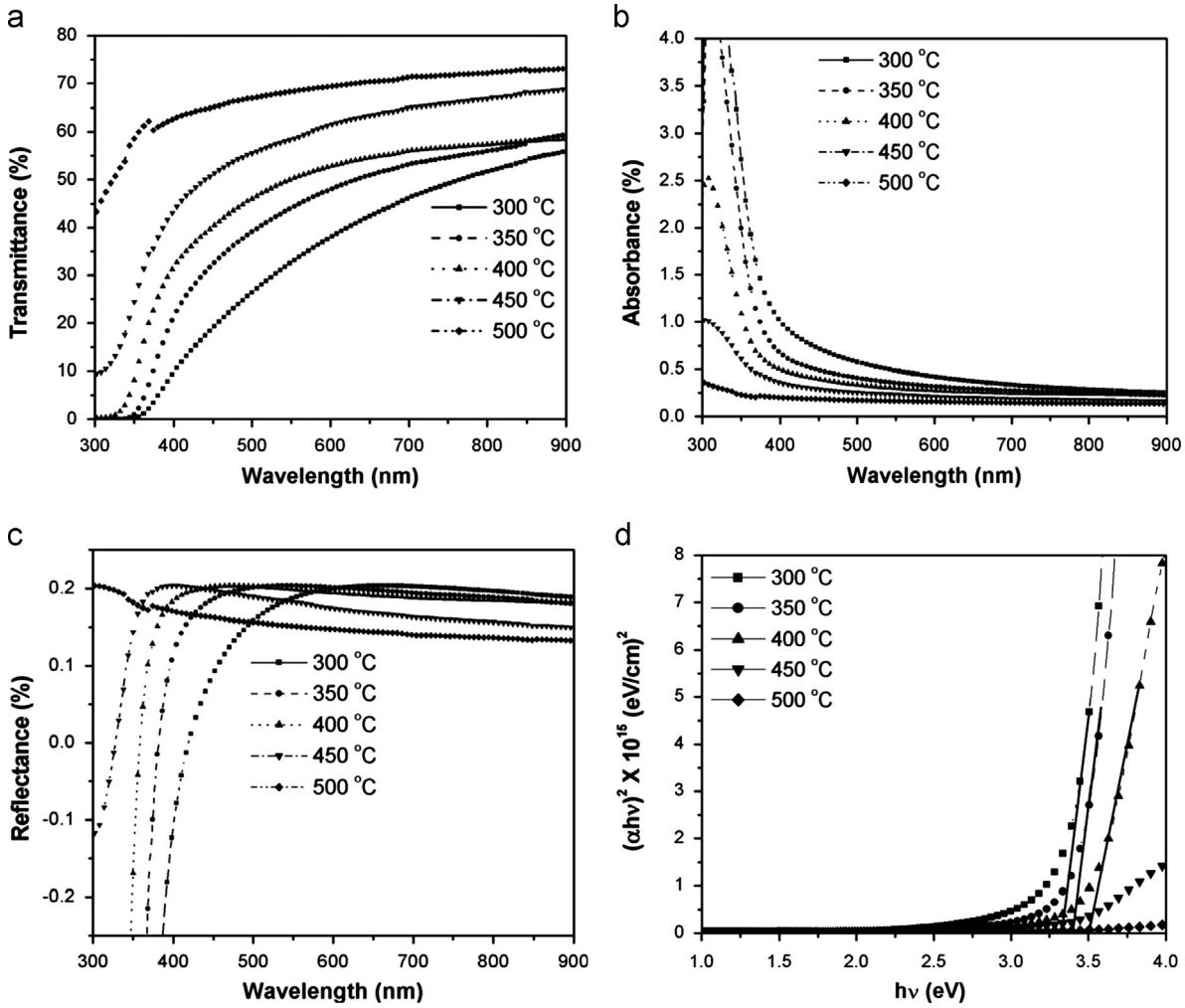

Fig. 1. Variations of (a) transmittance, (b) absorbance, (c) reflectance and (d) band gap energy spectra of CeO_2 thin films.

The refractive index (n) and extinction coefficient can be determined from the reflectance (R) data using the relation

$$n = \frac{1+R}{1-R} \pm \sqrt{\frac{4R}{(1-R)^2} - k^2} \quad (4)$$

$$PD = \frac{(n-n_i)}{(n_s-n_i)} \quad (5)$$

where R is the reflectance, PD is the packing density, n is the refractive index of the prepared sample, n_i is the refractive index of bulk material and n_s is the refractive index of solid.

The variation of refractive index and packing density of cerium oxide thin films with wavelength in the range 300–900 nm are shown in Fig. 2c and d. It shows that the refractive index of the films decreases sharply with increasing wavelength in the UV region and increases gradually in the visible region. Refractive index of the films are found to be increased with increasing substrate temperature up to 400 °C and then decreases due to the increase of packing density of the films and decrease of diameter of spray droplets. The maximum value of refractive index is calculated as 2.35. The above variations of the extinction coefficient and refractive index of the photon energy are similar to that reported by Mansilla et al. [26]. The absorption and extinction coefficient are found to be decreased with increasing substrate temperature due to the densification of the films and the film thickness [8]. The substrate temperature strongly affects the optical parameters like refractive index and packing density as listed in Table 1.

3.2. Structural properties

The X-ray diffraction spectra of CeO_2 films deposited at various substrate temperatures (300–500 °C) using pure aqueous solution of cerium nitrate are shown in Fig. 3. No other impurity peaks are observed due to the single phase nature of ceria films up to 400 °C; on close observation there is new impurity peak at $2\theta = 30.85$ (011) of Ce_2O_3 phase observed at 450 °C [35]. The film prepared at substrate temperature above 450 °C has amorphous nature due to the kinetic growth of the films and appearance of new Ce_2O_3 phase. As the substrate temperature increases, the films become more crystallite as indicated by the (200) peak with increased intensity and the corresponding FWHM is found to be decreased. When temperature reaches 350 °C, the preferred orientation changes to (200). The films are

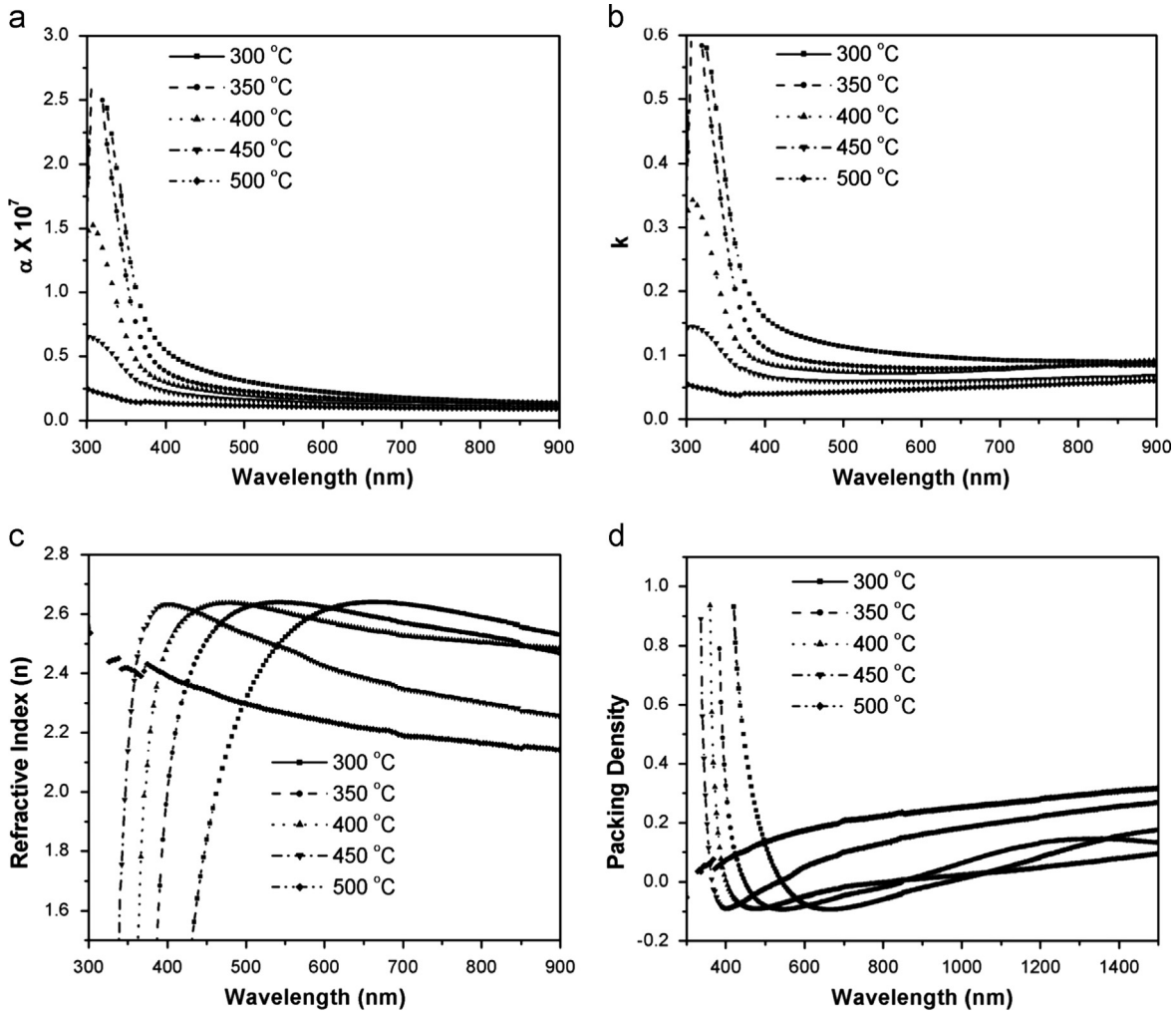

Fig. 2. Variations of (a) absorption coefficient, (b) extinction coefficient, (c) refractive index and (d) packing density with wavelength of CeO_2 thin films.

Table 1
Optical parameters of CeO_2 thin films.

Substrate temperature (°C)	α ($\times 10^6$)	k	Bandgap (eV)	Refractive index	Packing density	Thickness (nm)
300	2.45	0.109101	3.34	2.24	0.17	466
350	1.83	0.098367	3.41	2.30	0.12	442
400	1.67	0.081925	3.52	2.35	0.10	416
450	1.39	0.063242	3.35	2.08	0.27	386
500	1.08	0.040814	3.28	2.02	0.32	368

well crystallized in the cubic fluorite structure with preferred orientation along (200) reflection [2] compared to JCPDS data 34-0394. The substrate temperature strongly affects the growth of (111) and (200) peaks as shown in Fig. 3. A well-crystallized film is obtained at 400 °C and hence this substrate temperature is optimized for further fabrication.

The size of crystallites oriented along (111), (200), and (220) peaks were calculated with the help of Scherrer's relation:

$$D = \frac{k\lambda}{\beta \cos\ \theta} \tag{6}$$

The dislocation density and microstrain of the CeO_2 films were calculated from the following formula:

$$\delta = \frac{1}{D^2} \tag{7}$$

$$\varepsilon = \frac{\beta \cos\ \theta}{4} \tag{8}$$

$$SF = \left[\frac{2\pi^2}{45(3\tan\ \theta)^{(1/2)})}\right] \tag{9}$$

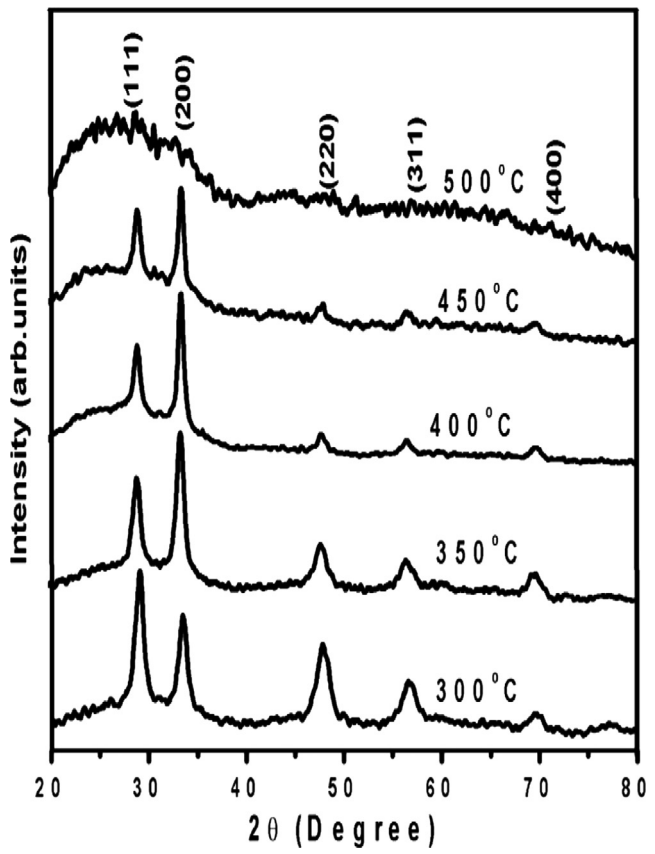

Fig. 3. XRD spectra of CeO_2 thin films with substrate temperatures: (a) 300 °C, (b) 350 °C, (c) 400 °C, (d) 450 °C and (e) 500 °C.

where k is the shape factor (0.94), λ is the wavelength of X-ray (1.5406 Å) and β is the full-width at the half-maximum of the (111), (200), and (220) peaks, θ is the Bragg angle of the XRD peak, δ is the dislocation density, ε is the microstrain and SF is the stacking fault. The crystallite size, dislocation density, microstrain, stacking fault and texture coefficient of the CeO_2 films are listed in Table 2. It is observed that (Table 2) the crystalline size increases when the temperature increases up to 400 °C, and then decreases. The maximum crystallite of the films is found to be 21, 19 and 11 nm for 400 °C. Due to the removal of defects in the lattice with increase in substrate temperature the microstrain and dislocation density in the films are released and attain a minimum value at 400 °C. Such a release in microstrain reduced the variation of interplanar spacing and thus leads to a decrease in dislocation density and stacking fault of the film (Table 2) and minimum values are obtained for films deposited at 400 °C. This decrease in microstrain, dislocation density and stacking fault improves the stoichiometry of the films which in turn causes the volumetric expansion of the films.

$$T_c = \frac{I_o(h_i k_i l_i)}{I_s(h_i k_i l_i)} \left[\frac{1}{N} \sum_{i=1} \frac{I_o(h_i k_i l_i)}{I_s(h_i k_i l_i)} \right]^{-1} \quad (10)$$

where T_c is the texture coefficient, I_o is the observed intensity and I_s the standard intensity and n is the reflection number. Calculated $T_c[h_i k_i l_i]$ values give us some important structural

Table 2
Structural parameters of CeO_2 thin films.

Temperature (°C)	2θ	d spacing (nm)	FWHM	hkl	Crystalline size (nm)	Dislocation density	Strain	Lattice constant (Å)	Stacking fault	Texture coefficient
300	29.066	3.0722	0.4546	111	18	0.00029	0.00195	5.3212	0.22589	0.6871
	33.5554	2.6707	0.6494	200	13	0.00051	0.0024	5.3415	0.29921	1.6263
	47.7418	1.9034	0.792	220	11	0.00049	0.00199	5.3838	0.30120	0.6865
350	29.0745	3.0713	0.4546	111	18	0.00029	0.00195	5.3197	0.22585	0.4432
	33.4349	2.6801	0.5845	200	14	0.00041	0.00217	5.3602	0.26982	2.2241
	47.7531	1.9030	1.1088	220	12	0.00095	0.00279	5.3826	0.42163	0.3325
400	29.0465	3.0742	0.3897	111	21	0.00022	0.00168	5.3247	0.19371	0.3868
	33.5346	2.6723	0.4546	200	19	0.00025	0.00168	5.3447	0.20953	2.7453
	48.0008	1.8953	0.7793	220	11	0.00047	0.00195	5.3609	0.29547	0.1811
	69.9139	1.3444	1.1088	400	12	0.00054	0.00177	5.3776	0.33550	0.6866
450	29.0449	3.0744	0.6494	111	13	0.0006	0.00279	5.325	0.32281	0.3950
	33.552	2.6710	0.5196	200	16	0.00032	0.00192	5.342	0.23942	2.4722
	47.8467	1.8995	0.9504	220	9	0.0007	0.00239	5.3727	0.36101	0.1327

information: (i) $T_c[h_ik_il_i]$ has to be bigger than 1 to determine the preferential orientation, (ii) if $T_c[h_ik_il_i]$ is approximately 1 for all the $[h_ik_il_i]$ planes considered at X-ray diffraction patterns, the films are randomly oriented, (iii) $T_c[h_ik_il_i]$ values higher than one indicate the abundance of grains in a given $[h_ik_il_i]$ direction and (iv) $0 < T_c[h_ik_il_i] < 1$ values indicate the lack of grains

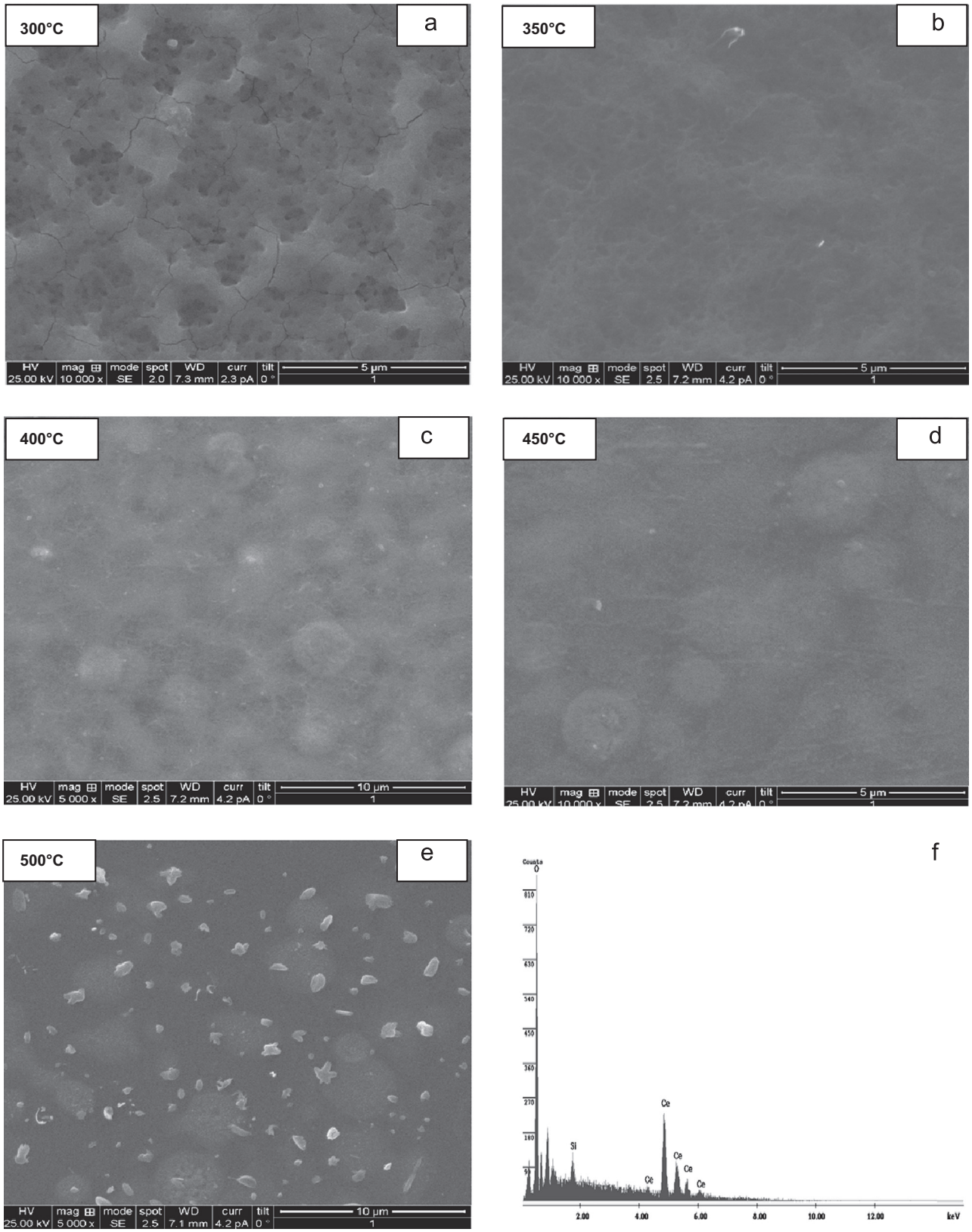

Fig. 4. SEM and EDX analyses of CeO_2 thin films.

oriented in that direction [37]. Subsequently $[h_ik_il_i]$ reflections corresponding to CeO_2 films were used in the texture coefficient calculations: (111), (200) and (220) directions. Table 2 summarizes the results of texture coefficient calculations for the observed $[h_ik_il_i]$ reflections in CeO_2 films at different temperatures. Note that the values of the texture coefficient of the high index plane (200) of the CeO_2 film are greater than unity while they are less than one for the low index (111) and (200) planes. The texture coefficient for the (200) plane increases significantly from 1.626 to 2.745 with the temperature increasing up to 400 °C and then decreased. This may be useful for the fabrication of optoelectronics device applications using CeO_2 films deposited at 400 °C.

3.3. Morphological analysis

Fig. 4a–e shows the SEM images of cerium oxide thin films for different substrate temperatures from 300 to 500 °C. SEM images of cerium oxide thin films prepared at 300 °C show some cracks with uneven surfaces due to the decomposition of unevaporated precursor spray droplets present in the heated substrates as shown in Fig. 4a. Films prepared at above 350 °C show the golf-ball like structure comprising small cracks and pores due to the shrinkage and compaction of spray droplets moving towards the substrates as shown in Fig. 4b–d. These spherical structures appear to retain the space inside and there are microvoids between golf-ball like structure and small pores [3]. Films prepared at 500 °C shows dense golf-ball like structure with some small crystallites as shown in Fig. 4e. The EDX spectrum of CeO_2 film prepared at 400 °C is shown in Fig. 4f. The EDX analysis confirmed the presence of Ce and O in the prepared films. The atomic ratio of Ce decreases with the increase of substrate temperature due to the coalescence of droplets and increases the oxygen vacancies of cerium oxide. The elemental compositions of the prepared samples are listed in Table 3.

3.4. I–V characteristics

Four-probe resistivity method is used to study the electrical properties of cerium oxide thin films deposited at different substrate temperatures using Keithley Electrometer 6517 B. The resistivity is measured in air atmosphere. The variations of resistivity and conductivity with substrate temperature for the CeO_2 film are shown in Fig. 5. The resistivity of all the films decreases with increasing substrate temperature up to 400 °C

Table 3
Elemental composition of CeO_2 thin films.

Substrate temperature (°C)	Ce (at%)	O (at%)	Si (at%)
300	18.76	77.56	3.68
350	17.50	69.19	13.31
400	12.06	61.15	26.80
450	2.92	60.16	36.92
500	0.35	62.64	37.01

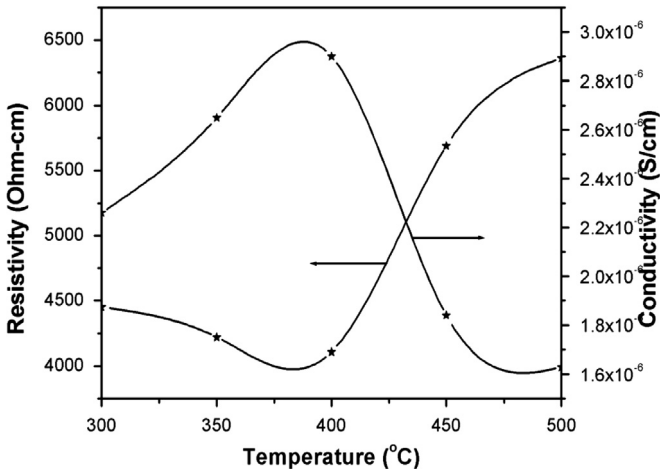

Fig. 5. Variations of resistivity and conductivity of CeO_2 thin films.

Table 4
Electrical properties of CeO_2 thin films.

Substrate temperature (°C)	Resistivity (Ω cm)	Conductivity ($\times 10^{-6}$ S/cm)
300	4498	2.45
350	4258	2.72
400	4162	2.90
450	5502	1.86
500	6250	1.65

and then increases which is due to the new phase of Ce_2O_3. The conductivity is calculated and found to be varied in the range 1.65×10^{-6}–2.90×10^{-6} S/cm for different substrate temperatures as listed in Table 4.

3.5. XPS analysis

XPS is a straightforward and nondestructive technique for the investigation of chemical and electronic structures of materials. An important advantage of XPS is its ability to characterize the variations in the binding energies of the core level or chemical shifts of the samples. Fig. 6a shows the survey spectrum of CeO_2 thin films in the binding energy range 0–1000 eV. Only three elements are detected on the surface of the film as cerium, oxygen and also some carbon showing the photoelectron peaks Ce 3d, Ce 4d for cerium, O 1s, O 2p for oxygen and C 1s for carbon. Ce 3d core level spectra clearly show the five spin–orbit-split doublets of binding energies at 890.19 eV, 896.73 eV, 906.45 eV, 908.15 eV and 916.42 eV as shown in Fig. 6b [3]. The first two peaks correspond to Ce $3d_{5/2}$ and last three peaks correspond to Ce $3d_{3/2}$. These results indicate the presence of pure CeO_2 and no other impurities are presented like Ce_2O_3. This is further supported by the presence of peak at 916.42 eV, which is considered as a fingerprint of the CeO_2 phase [38]. Ce 4d core level spectra clearly show the five peaks of binding energies at 114.59 eV, 117.79 eV, 120.99 eV, 125.37 eV and 127.87 eV as shown in Fig. 6c. The first three peaks

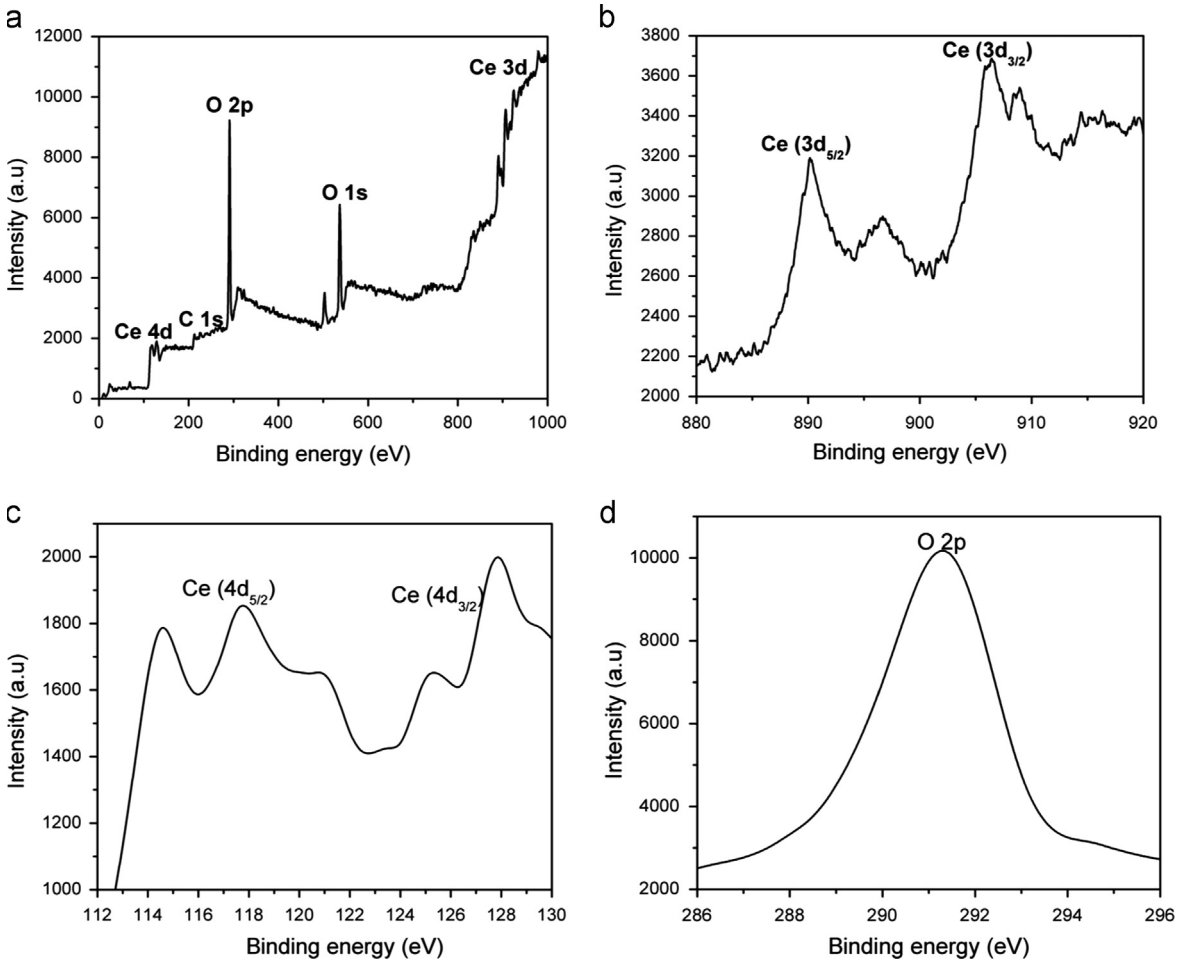

Fig. 6. XPS spectra of CeO_2 thin films.

correspond to Ce $4d_{5/2}$ and the last two peaks correspond to Ce $4d_{3/2}$. Fig. 6d–f shows the O 2p, O 1s and C 1s core level spectra of CeO_2 thin films. Oxygen atom is presented in two oxidation states O 2p and O 1s at binding energies 291.23 eV and 536.69 eV respectively. Small amount of carbon atom is absorbed from atmosphere at binding energy 291.98 eV [39]. These results conclude the presence of single phase nature of CeO_2 thin films with no other impurities.

$$[Ce^{3+}] = \frac{Ce^{3+}}{Ce^{3+} + Ce^{4+}} \quad [Ce^{4+}] = \frac{Ce^{4+}}{Ce^{3+} + Ce^{4+}} \tag{11}$$

The calculations led to the fact that these ceria thin films have 5.8% of carbon, 41.8% of oxygen, 21.8% of Ce^{3+} and 30.4% of Ce^{4+}.

4. Conclusion

Nanocrystalline, uniform and crack-free cerium oxide thin films are successfully deposited on glass substrates by simple and low cost effective nebulizer spray pyrolysis technique at different substrate temperatures using cerium nitrate as the source material. All films are found to be single phase and well crystalline with most prominent (200) reflection. Crystallinity of the film is found to be increased with increasing substrate temperature up to 400 °C which then decreases. The calculated crystalline size is found to be varied in the range 9–21 nm. Optical analysis revealed that the films are highly transparent (70%) in the visible region. The high refractive index and bandgap is observed as 2.35 and 3.52 eV respectively. SEM images exhibits the formation of uniform and porous films with golf-ball like structure. The conductivity lies in the range $1.65–2.90 \times 10^{-6}$ S/cm. The best film is formed at 400 °C with better crystallinity, high refractive index and smooth morphology. Substrate temperature strongly affects the optical, structural and electrical properties of CeO_2 films due to the decrease of sprayed droplet diameter, presence of unevaproated precursor and densification of the films.

References

[1] Shengyne Wang, Wei Wang, Qiangchun Liu, Min Zhang, Yitai Qian, Preparation and characterization of cerium (IV) oxide thin films by spray pyrolysis method, Solid State Ionics 133 (2000) 211–215.
[2] B. Elidrissi, M. Addou, M. Regragui, C. Monty, A. Bougrine, A. Kachouane, Structural and optical properties of CeO_2 thin films prepared by spray pyrolysis, Thin Solid Films 379 (2000) 23–27.
[3] A.K. Bhosale, N.L. Tarwal, P.S. Shinde, P.M. Kadam, R.S. Patil, S.R. Barman, P.S. Patil, Effective utilization of spray pyrolyzed CeO_2

as optically passive counter electrode for enhancing optical modulation of WO_3, Solid State Ionics 180 (2009) 1324–1331.
[4] W. Pinc, P. Yu, M.O. Keefe, W. Fahrenholtz, Effect of gelatin additions on the corrosion resistance of cerium based conversion coatings spray deposition on Al 2024-T3, Surface and Coating Technology 203 (2009) 3533–3540.
[5] T. Hirai, H. Koike, K. Nagashima, Y. Tarui, K. Teramoto, Characterization of metal/ferroelectrics/insulator/semiconductor structure with CeO_2 buffer layers, Japanese Journal of Applied Physics 34 (1995) 4321–4324.
[6] S.M.A. Durrani, M.F. Al-Kuhaili, I.A. Bakhtiari, Carbon monoxide gas-sensing properties of electron-beam deposited cerium oxide thin films, Sensors and Actuators B 134 (2008) 934–939.
[7] Syed M. Bukhari, Javier B. Giorgi, Electrical conductivity dependence of Ni doped $Sm_{0.95}Ce_{0.05}FeO_{3-\delta}$ on surface morphology and composition, Sensors and Actuators B 156 (2011) 524–537.
[8] F.E. Ghodsi, F.Z. Tepehan, G.G. Tepehan, Optical and structural properties of sol–gel made Ce/Ti/Zr mixed oxide thin films as transparent counter electrode for electrochromic devices, Optical Materials 31 (2008) 63–67.
[9] A.K. Bhosale, P.S. Shinde, N.L. Tarwal, R.C. Pawar, P.M. Kadam, P.S. Patil, Synthesis and characterization of highly stable optically passive CeO_2–ZrO_2 counter electrode, Electrochimica Acta 55 (2010) 1900–1906.
[10] A.K. Bhosale, P.S. Shinde, N.L. Tarwal, P.M. Kadam, S.S. Mali, P.S. Patil, Synthesis and characterization of spray pyrolyzed nanocrystalline CeO_2–SiO_2 thin films as passive counter electrodes, Solar Energy Materials and Solar Cells 94 (2010) 781–787.
[11] H. Sato, H. Akoh, S. Takada, R. Miyagawa, YBaCuO multilayer structures using CeO_2 insulating films, IEEE Transactions on Applied Superconductivity 7 (1997) 2165–2168.
[12] T. Petrisor, V. Boffa, G. Celentano, L. Ciontea, F. Fabbri, U. Gambardella, S. Ceresara, P. Scardi, Development of biaxially aligned buffer layers on Ni and Ni-based alloy substrates for YBCO tapes fabrication, IEEE Transactions on Applied Superconductivity 9 (1999) 2256–2259.
[13] B.B. Patil, S.H. Pawar, Spray pyrolytic synthesis of samarium doped ceria ($Ce_{0.8}Sm_{0.2}O_{1.9}$) films for solid oxide fuel cell applications, Applied Surface Science 253 (2007) 4994–5002.
[14] Ji-Guang Li, Takayasu Ikegami, Toshiyuki Mori, Low temperature processing of dense samarium-doped CeO_2 ceramics: sintering and grain growth behaviors, Acta Materialia 52 (2004) 2221–2228.
[15] A. Samson Nesaraj, I. Arul Raj, R. Pattabiraman, Synthesis and characterization of $LaCoO_3$ based cathode and its chemical compatibility with CeO_2 based electrolytes for intermediate temperature solid oxide fuel cell (ITSOFC), Indian Journal of Chemical Technology 14 (2007) 154–160.
[16] V. Thangadurai, W. Weppner, $Ce_{0.8}Sm_{0.2}O_{1.9}$: characterization of electronic charge carriers and application in limiting current oxygen sensors, Electrochimica Acta 49 (2004) 1577–1585.
[17] H.Z. Song, H.B. Wang, S.W. Zha, D.K. Peng, G.Y. Meng, Aerosol-assisted MOCVD growth of Gd_2O_3-doped CeO_2 thin SOFC electrolyte film on anode substrate, Solid State Ionics 156 (2003) 249–254.
[18] Ulrich P. Muecke, Kcjiro Akiba, Anna Infortuna, Tomas Salkus, Nataliaya V. Stus, Ludwig J. Gauckler, Electrochemical performance of nanocrystalline nickel/gadolinia-doped ceria thin film anodes for solid oxide fuel cells, Solid State Ionics 178 (2008) 1762–1768.
[19] Lin Liu, Gap-Yong Kim, Abhijit Chandra, Fabrication of solid oxide fuel cell anode electrode by spray pyrolysis, Journal of Power Sources 195 (2010) 7046–7053.
[20] J.R. Vargas-Garcia, L. Beltran-Romero, R. Tu, T. Goto, Highly (100)-oriented CeO_2 films prepared on amorphous substrates by laser chemical vapor deposition, Thin Solid Films 519 (2010) 1–4.
[21] L.R. Pederson, P. Singh, X.D. Zhou, Application of vacuum deposition methods to solid oxide fuel cells, Vacuum 80 (2006) 1066–1083.
[22] Jong Hoon Joo, Gyeong Man Choi, Electrical conductivity of YSZ film grown by pulsed laser deposition, Solid State Ionics 177 (2006) 1053–1057.
[23] Irena kozjek Skofic, Saso Sturm, Miran Ceh, Natasa Bukovec, CeO_2 thin films obtained by sol–gel deposition and annealed in air or argon, Thin Solid Films 422 (2002) 170–175.
[24] Ming Wei, K.L. Choy, Deposition of cerium oxide films on Si (100) and glass substrates using the ESAVD method, Journal of Crystal Growth 284 (2005) 464–469.
[25] Yinzhu Jiang, Naoufal Bahlawane, Changes in the structural and optical properties of CeO_2 nanocrystalline films: effect of film thickness, Journal of Alloys and Compounds 485 (2009) L52–L55.
[26] Catalina Mansilla, Structure, microstructure and optical properties of cerium oxide thin films prepared by electron beam evaporation assisted with ion beams, Solid State Sciences 11 (2009) 1456–1464.
[27] Giedrius Laukaitis, Mindaugas Jauncika, Julius Dudonis, Oresta Katkauske, Darius Milcius, The properties of samarium doped ceria oxide thin films grown by e-beam deposition technique, Vacuum 83 (2009) S114–S117.
[28] Nikolaous I. Karageorgakis, Andre Heel, Thomas Graule, Ludwig J. Gauckler, Flame spray deposition of nanocrystalline dense $Ce_{0.8}Gd_{0.2}O_{2-\delta}$ thin films: deposition mechanism and microstructural characterization, Solid State Ionics 192 (2011) 464–471.
[29] K. Konstantinov, I. Stambolova, P. Peshev, B. Darriet, S. Vassilev, Preparation of ceria films by spray pyrolysis method, International Journal of Inorganic Materials 2 (2000) 277–280.
[30] B. Elidrissi, M. Addou, M. Regragui, A. Mzerd, A. Bougrine, A. Kachouane, Solid State Ionics 140 (2001) 369–374.
[31] Shengyne Wang, Wei Wang, Jian Zuo, Yitai Qian, Study of the Raman spectrum of CeO_2 nanometer thin films, Materials Chemistry and Physics 68 (2001) 246–248.
[32] N.L. Petrova, R.V. Todorovska, D.S. Todorovsky, Spray-pyrolysis of CeO_2 thin films using citric or tartaric complexes as starting materials, Solid State Ionics 177 (2006) 613–621.
[33] M.G. Chourashiya, S.H. Pawar, L.D. Jadhav, Synthesis and characterization of $Ce_{0.9}Gd_{0.1}O_{1.95}$ thin films by spray pyrolysis technique, Applied Surface Science 254 (2008) 3431–3435.
[34] S. Debnath, M.R. Islam, M.S.R. Khan, Optical properties of CeO_2 thin films, Bulletin of Materials Science 30 (2007) 315–319.
[35] B.B. Patil, S.H. Pawar, Structural, morphological and electrical properties of spray deposited nano-crystalline CeO_2 thin films, Journal of Alloys and Compounds 509 (2011) 414–420.
[36] P.S. Patil, Versatility of chemical spray pyrolysis technique, Materials Chemistry and Physics 59 (1999) 185–198.
[37] R. Mariappan, V. Ponnuswamy, M. Ragavendar, Growth and characterization of chemical bath deposited CdZnS thin films, Journal of Alloys and Compounds 509 (2011) 7337–7343.
[38] A. Trinchi, Y.X. Li, W. Wlodarski, S. Kaciulis, L. Pandolfi, S. Viticoli, E. Comini, G. Sberveglieri, Investigation of sol–gel prepared CeO_2–TiO_2 thin films for oxygen gas sensing, Sensors and Actuators B 95 (2003) 145–150.
[39] J.L.M. Rupp, T. Drobek, A. Rossi, L.J. Gauckler, Chemical analysis of spray pyrolysis gadolinia-doped ceria electrolyte thin films for solid oxide fuel cells, Chemistry of Materials 19 (2007) 134–142.